Heliyon 8 (2022) e10308

Contents lists available at ScienceDirect

Heliyon

journal homepage: www.cell.com/heliyon

Research article

Anthropomorphic Polydimethylsiloxane silicone-based phantom for Diffuse Optical Imaging

M.V. Waks Serra [a,*], V. Noseda Grau [b], D.A. Vera [a], S. Jodra [b], H.A. García [a], N.A. Carbone [c], P.A. Pardini [c], J.A. Pomarico [a], D.I. Iriarte [a]

[a] CIFICEN (UNCPBA - CICPBA - CONICET), Pinto 399, 7000, Tandil, Argentina
[b] IFIMAT (UNCPBA), Pinto 399, 7000, Tandil, Argentina
[c] BIONIRS Arg SA, Fugl 855 Dpto 12, 7000, Tandil, Argentina

HIGHLIGHTS

- We constructed anthropomorphic phantoms for Diffuse Optical Imaging.
- They simulate the optical and mechanical characteristics of a human breast.
- A new scattering agent was successfully introduced.
- Results of Diffuse Optical images are compared to Ultrasound images.

ARTICLE INFO

Keywords:
PDMS phantom
Diffuse optical imaging
Mammography

ABSTRACT

This work presents a method for constructing phantoms suitable for diffuse optical mammography. They are based on Polydimethylsiloxane silicones, with the characteristic of being anthropomorphic, and having similar mechanical and optical properties as a real breast. These phantoms are useful for testing the performance of diffuse optical imaging devices in the near infrared, both in transmittance and reflectance geometries, since they can be constructed containing inclusions, to simulate breast tumors. An alternative component to be used as scattering agent, that is easier to handle than traditional scattering agents, is also studied.

The optical properties of the phantoms were tested varying the concentration of scattering and absorbing agents, while their mechanical properties were modified by adding a silicone fluid to the basic mixture.

Finally, the phantoms were tested by Diffuse Optical Imaging experiments, and these images were compared to the ones obtained by conventional ultrasound techniques.

Results show that the constructed anthropomorphic phantoms properly reproduce the optical and mechanical characteristics of human breasts, and are suitable to be used in Diffuse Optical Imaging.

1. Introduction

The use of near infrared light as a medical imaging tool has been a subject of study for the last four decades. The associated technique is known as Near Infrared Spectroscopy (NIRS) and it is capable of complementing other well established techniques such as X-Rays or ultrasound, specially for performing studies on soft, diffusive tissues, like breasts [1, 2, 3, 4]. It has been found useful because it provides valuable complementary clinical information, such as composition (concentration of hemoglobin, lipids, collagen, etc.) [5, 6] and tissue oxygenation [7, 8]. Moreover, research has advanced to the point of designing and testing clinical prototypes [9, 10, 11, 12, 13, 14]. In this way, the development of devices intended for clinical applications, such as early detection, diagnosis, or measurements of response to therapy, is one of the main research goals in Biomedical Optics. Because of all this, it is imperative to count with suitable and durable phantoms to perform tests [15], whether in prototypes or in the laboratory, as well as in the control and calibration of some types of devices used in the clinics. These phantoms have the function of reproducing, with different materials, the physical and optical characteristics of tissues interacting with

* Corresponding author.
E-mail address: mvwaks@ifas.exa.unicen.edu.ar (M.V. Waks Serra).

https://doi.org/10.1016/j.heliyon.2022.e10308
Received 23 February 2022; Received in revised form 6 July 2022; Accepted 11 August 2022

light and thus, they can be used either to compare results from different measurement approaches and algorithms or to track the performance of NIRS devices during their development under controlled experimental conditions.

In recent years the challenge has been to develop phantoms that meet not only the optical properties, but also have characteristics which adapt to different imaging modalities. That is, they include in their preparation the use of different chromophores (biologically compatible if possible), and variations in their concentrations of water, lipids, collagen and hemoglobin. In the case of NIRS or Diffuse Optical Imaging (DOI), several kinds of phantoms have been proposed [16], and they are commonly elaborated with epoxy resins [17, 18] or Polydimethylsiloxane (PDMS) silicones [19, 20, 21, 22]. Also, milk or Intralipid (IL) phantoms have been used before [23, 24], either liquid (consisting of milk or IL, water and an absorbing agent) or solid (with the addition of gelatin, agar or agarose powders) [23, 25, 26]. These milk based phantoms are versatile, of simple elaboration and their optical properties can be easily tuned, making them very useful for experiments where optical parameters need to be varied. However, their main disadvantage is that their lifetime is quite short, even if properly stored at low temperature. On the other hand, although resin or silicone phantoms are more difficult to construct with the required optical parameters, they can be reused over long periods of time without modifying their initial properties.

Additionally, it is usual to construct both, liquid and solid phantoms with flat surfaces. This is a very useful approach that simplifies measurements and preserves the nominal locations of the previously embedded inclusions. However, tests on clinical devices, and in particular those intended to emulate human breasts, may require phantoms that reproduce not only their optical properties, but also their shape and stiffness. In this way, it would be possible to consider the effects of compression and edges, and thus to reproduce, in a realistic way, clinical situations where the simulated tumors may be more difficult to detect with optical methods.

With all that in mind, in this work we develop and test anthropomorphic, human breast-shaped silicone phantoms (homogeneous and with inclusions) with variable hardness, and containing different concentrations of the scattering and absorbing components, to be applied in DOI. Flat cylindrical phantoms have been also constructed for comparison purposes. Moreover, white acrylic paint is introduced as an alternative scattering agent in replacement of the usual titanium dioxide (TiO_2) [19, 27].

The paper is organized as follows: in Section 2, Methods and Materials, the procedure of construction of the phantoms, the materials used, and the characterization techniques, are detailed. Section 3 describes the main results and their discussion. Finally, in Section 4, the most important conclusions are given.

2. Methods and materials

2.1. General considerations

Polydimethylsiloxane (PDMS), commercially known as “silicone”, is an optically clear, non-toxic, and non-flammable polymer. Its applications range from the fabrication of contact lenses and medical devices to the elaboration of elastomers [28]. In general, PDMS is transparent at optical wavelengths in the range from 240 nm to 1100 nm [20]. However, some differences may appear depending on brand and model, and some silicones present an absorption peak at 900 nm. For manufacturing the phantoms, Silcast 815 (Novarchem, Argentina) was selected, a platinum-catalyzed silicone rubber with a Shore hardness of 15. These systems consist of two components: A (the silicone) and B (the curing agent), which are to be mixed in equal quantities by weight or volume, and cured at room temperature, presenting negligible shrinkage. Besides, to allow the construction of phantoms with variable hardness, a silicone fluid (Silcast Fluid, Novarchem, Argentina) was added to the two principal components. This non-reactive silicone fluid lowers the viscosity of the silicone rubber, and thus the hardness of the cured product. Fig. 1 shows a plot of the absorption spectrum, obtained using a spectrophotometer Shimadzu UV-1800, of the selected material as a function of wavelength in the range from 240 nm to 1100 nm. Despite the fact that a small absorption peak can be seen at 900 nm, very low absorption occurs within the whole NIR range. Although in our work this wavelength is not used, this phenomenon should be considered if the phantom is going to be measured at 900 nm, and thus, the proportion of absorbing agent should be adjusted in accordance.

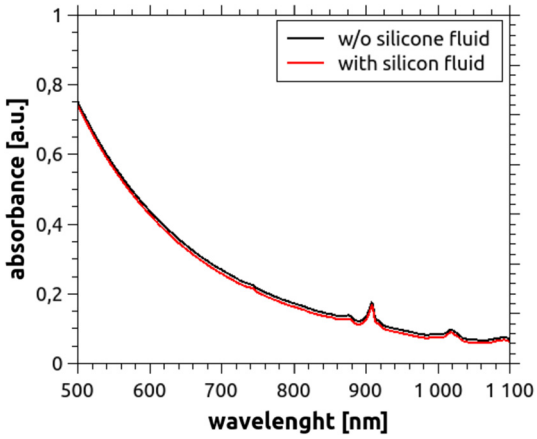

Fig. 1. Absorbance plot of Silcast 815, the silicone used in this work. It was measured without silicone fluid (black solid line) and for three different concentrations of the diluting fluid, namely 20%, 40% and 60% (weight percentage). No significant differences occur for these concentrations. Thus, only the curve for 60% (solid red) is shown, since it corresponds to the one which best reproduces the stiffness of a real breast. An absorption peak at 900 nm can be clearly seen.

As light absorbing agent, black toner from laser printers was used. This material is commonly used for silicone and resin phantoms, and thus, its behavior is well known [17, 18]. Since it consists of very small particles, prone to agglutinate due to static electricity, and the needed amount is very small, a previous dilution of toner in part A of the PDMS system was made.

Regarding the scattering agent, although titanium dioxide (TiO_2) is the most common material used, it presents several problems that hinder the reproducibility of the obtained phantoms, since it is difficult to be evenly distributed in the mixture and tends to create clusters which sediment at the bottom [16]. Several mechanisms to incorporate TiO_2 to the silicone were attempted, such as high RPM mixers and long sonication times with different degrees of success. To avoid the cumbersome procedures required by TiO_2, white acrylic paint (Monitor, number 801 “Titanium White”, Argentina) was used as an alternative scattering agent. It showed to simultaneously satisfy the desired conditions, namely: it mixes very well and easily with the silicone, and the optical properties obtained are consistent and reproducible for the different constructed phantoms. The absorbance of this new material was measured in the spectral range that is of interest for Biomedical Optics, using the spectrophotometer Shimadzu UV-1800. In Fig. 2 it can be seen that it has a flat peak around 550 nm, and its absorbance decreases almost linearly between 600 nm and 1000 nm.

Homogeneous Phantoms

For the fabrication of the phantoms, the general guidelines reported by Ayers et al. [19] were followed, although due to the difference in the silicone model and the chosen scattering agent, some procedures were modified. The concentration of both scattering and absorbing agents were selected to achieve optical properties similar to those of a healthy human breast, i.e. $\mu_a = 0.01\ \text{mm}^{-1}$ and $\mu_s' = 1\ \text{mm}^{-1}$ [29].

The whole fabrication process can be summarized in the following steps:

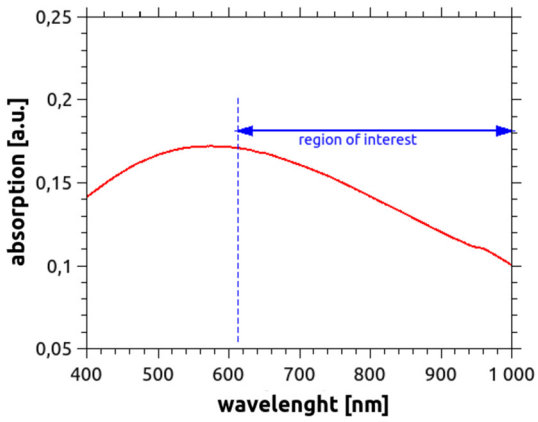

Fig. 2. Absorbance of white acrylic paint, diluted in water, in a concentration of 3.5×10^{-5} g/ml.

- Part A of the silicone was weighed in a disposable container together with the required amounts of diluted toner and silicone fluid. Correspondingly, on a different disposable container, the same amount of part B and the needed proportion of acrylic paint were weighed.
- Both compounds were mixed separately for approximately 10 minutes using a high-rpm mixer. They were placed in a vacuum desiccator in order to evacuate air bubbles generated during the mixing process.
- These two previous preparations were then combined and thoroughly mixed for several minutes, again using a high-rpm mixer, and placed in the vacuum chamber.
- The final completed mixture was poured in the selected mold (previously waxed to help removing the phantom from it once cured) and let to solidify at 20 °C for at least 24 hours.

The adding of the silicone fluid has the advantage of making the silicone less viscous, which, in turn, delays the solidification and also helps in the evacuation of air bubbles.

Two different types of molds were employed: a cylindrical one, of 11 cm diameter, constructed with a 3D printer, and a second one, consisting in a breast-shaped brassiere manikin.

Phantoms containing inclusions

Inhomogeneous phantoms were constructed by embedding inclusions in the homogeneous ones. Three types of materials were used for making the inclusions, namely silicone, resin and 3D printers polylactic acid thermoplastic (PLA).

Silicone inclusions consisted of small cylinders of 9 mm diameter and 12 mm height; these were made following the procedure described previously. However, since breast tumors have a higher stiffness than the healthy tissue [30], the use of silicone fluid was omitted. Also, more absorbing agent (toner) was added to the preparation, in order to obtain an increased absorption relative to the background medium, thus mimicking the case of a malignant breast tumor [29]. A rectangular slab of $110 \times 70 \times 25$ mm^3 was also created from the same mixture to allow measurement of the optical properties. To construct the anthropomorphic phantom, the breast shaped mold was taken with the nipple down and the inclusion (or inclusions) was (were) placed inside it, hold by a spanned thread at a depth of 10 to 25 mm, measured from the top surface, and the original (bulk) silicone preparation was poured in it.

Another set of cylindrical and breast-shaped phantoms was constructed containing resin inclusions of appropriate optical properties. These inclusions were made following the guidelines described in [31, 32]. Briefly, the process consists in making rectangular slabs, whose optical properties are measured, and then machine-lathing them into spheres, with diameters between 6 mm and 13 mm; these resulted in volumes between 113 and 1150 mm^3.

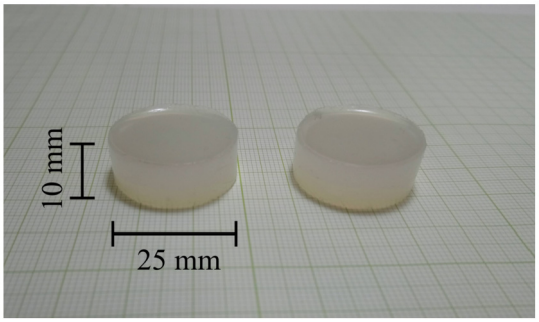

Fig. 3. Cylindrical silicone samples used to test the variation of the hardness with the adding of silicone fluid.

A third set of phantoms was made, containing a completely black plastic inclusion (built in a 3D printer, using black PLA), considered as a "best case scenario", i.e. a situation where the inclusion can be easily detected with DOI.

2.2. Measurement of optical properties

Optical properties of the resulting phantoms were measured by time resolved (TR) techniques. First, a transmittance geometry was used for determining the optical properties of each inclusion (see previous section), and for studying the behavior of the optical properties of the phantoms for different amounts of absorbing and scattering agents. Second, the reflectance geometry was employed to obtain the optical properties of the cylindrical and anthropomorphic bulk phantoms.

For the TR measurements, a Time-Correlated Single Photon Counting (TCSPC) board (Becker & Hickl SPC 130) was used, together with a photomultiplier tube (Becker & Hickl PMC-100-20). A semiconductor laser (Becker & Hickl, BHLP-700), $\lambda = 785$ nm, operating at an average power of 2 mW and at 50 MHz repetition rate, producing 70 ps pulses was used as the light source. Its beam was delivered into the phantom via a 600 μm diameter multimodal optical fiber (Thorlabs, NA = 0.39). For the transmittance measurements, a 3 mm diameter optical fiber (Dolan Jenner, USA, NA = 0.55) was placed aligned with the source fiber at the opposite face of the slab; this detection fiber carries the emerging light to a photo-multiplier (PMT).

For the case of diffuse reflectance measurements, the 3 mm diameter collecting fiber was placed on the same face of the phantom and at a distance $\rho = 30$ mm from the illuminating fiber. Every time a photon is detected, the PMT sends an electrical pulse to the TCSPC board where the histogram of the times of arrival of the photons is built up [33]. From these Distribution of Times of Flight (DTOF), the optical properties can be inferred by fitting the data to the appropriate slab or semi-infinite model [34]. The refractive index of the silicone was measured, using a digital refractometer (Milwaukee Ma871), resulting in $n = 1.39 \pm 0.02$.

2.3. Measurement of the mechanical properties

Since one of the goals of these phantoms is to reproduce the mechanical behavior of a real breast, the elastic properties were measured, following the approach by Lamouche et al. [35] and Ismail et al. [36]. To this end, five cylindrical test samples, each of 25 mm diameter and 10 mm height, were fabricated for five different concentrations of silicone fluid (i.e., different stiffnesses), namely: 0%, 10%, 20%, 40% and 60%, and without absorbing agent. This process was repeated with the addition of the scattering agent in a concentration of 8 mg per gram of silicone, which is a concentration that produces a scattering coefficient similar to that of a healthy breast. A couple of these cylinders is shown in Fig. 3 as illustration.

The mechanical properties were measured using a universal testing machine (Shimadzu Autograph DSS-10T-S). In the compression test,

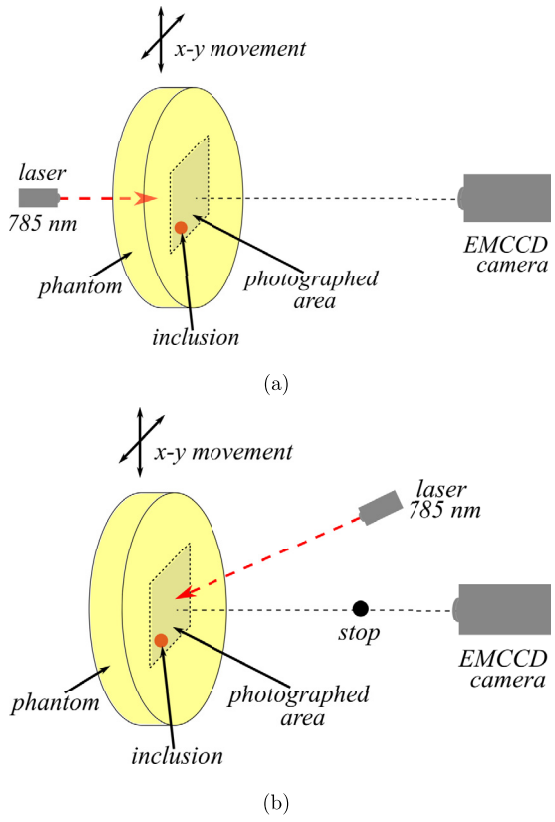

Fig. 4. Experimental setup used to obtain (a) transmittance and (b) reflectance images of the phantoms.

each sample was located between the plates of the machine (twice the transverse section of the samples) and controlled pressure was applied. To assure the proper contact between the plates and the sample, a pre-charge of 50 g was applied for 30 s. After this, the silicone was compressed at constant rate of 1 mm/minute until reaching 25% of deformation. To avoid transverse efforts, high density oil was used between the silicone sample and the compression cell.

2.4. Imaging experiments

The phantoms were analyzed with two imaging techniques: i) Diffuse Optical Imaging (DOI) and ii) ultrasound (US). For this last one, a commercial clinical device (General Electric Logiq F8) was used and the measurements were done by an experienced physician at a diagnostics center following the standard procedure for this technique.

The DOI experiments were performed by continuous wave diffuse transmittance and reflectance, following the procedures reported by Waks Serra et al. [24] and Carbone et al. [32]. The corresponding experimental setups are shown in Figs. 4 (a) and (b) for transmittance and reflectance geometries, respectively. For both cases, a CW laser (Thorlabs L785P25), operating at $\lambda = 785$ nm, was focused on one face of the phantom and images were taken by an EMCCD camera (Andor iXon Ultra 897). Images were acquired at several different positions by changing the illumination point moving the phantom horizontally and vertically by a two axes motorized translation stage (Zaber Technologies T-G-LSM200A). A background image was constructed averaging all these images. Each raw image was then divided by the background, for normalization.

For the transmittance geometry, the camera imaged the face of the phantom opposite to the illumination point (as seen in Fig. 4(a)). For the reflectance experiments, the camera looked at the same face being illuminated; also a small black stop was placed between the phantom and the camera to avoid saturation by the laser spot (see Fig. 4(b)).

Fig. 5. Photos of the resulting phantoms. (a) cylindrical, with a diameter of 100 mm and a thickness of 40 mm, and (b) breast-shaped.

Table 1. List of the constructed phantoms. *C* refers to a cylindrical phantom and *A* is used for the anthropomorphic ones. Note that phantom *A*1 contains no inclusions, i.e., it was constructed just for control purposes. Sizes and depths of the inclusions were chosen to lie inside the detectability limits for DOI (see for example [32]). Diameters and depths are given in mm.

Name	Nr incl	Inclusion	Diameter	Depth	$\mu_{aInclusion}/\mu_{aBulk}$
C1	1	black PLA	10	10	>10
C2	2	resin	10 - 13	10 - 20	1.8
C3	2	resin	10 - 10	10 - 20	3
A1	0	-	-	-	
A2	1	black PLA	10	19	>10
A3	1	silicone	9	26	2.4
A4	1	silicone	9	12	5
A5	2	resin	13 - 6	18.4 -20.5	1.43 - 2

Each anthropomorphic phantom was compressed between two transparent glass sheets in order to achieve a plane surface to be imaged by the camera. The cylindrical ones were simply kept in place by a plastic frame.

3. Results and discussions

Several phantoms emulating both, healthy and pathological-like breasts, were elaborated and characterized following the procedures described in Section 2. Fig. 5 shows examples of both, cylindrical (a) and anthropomorphic (b) phantoms.

Fig. 6 shows the three different types of inclusions that were embedded inside the phantoms. Several combinations of phantom shapes and inclusion types were elaborated. In Table 1, a summary of all the made phantoms is detailed.

In the following subsections, the results of testing the optical and mechanical characteristics of the materials are shown, as well as the images obtained by US and DOI techniques.

3.1. Optical properties

As a new scattering agent was introduced, it is important to verify the reproducibility of the optical properties achieved in the phantoms when it is used. To this end, four slabs were constructed by preparing independent mixtures following the same recipe (i.e. adding the same amount of scattering and absorbing agents). The concentration of the absorbing agent was kept constant and set to reproduce the absorption coefficient of healthy tissue, while three concentrations of the scattering agent were considered: one aiming to reproduce the reduced scattering coefficient of healthy tissue ($\mu_s' = 1$ mm^{-1}), one to achieve twice this value, and a last one to obtain half the reduced scattering coefficient of healthy tissue. The resulting optical properties, measured using the TCSPC technique described in Section 2.2, are plotted in Fig. 7 as a function of the sample number.

The second test consisted in determining the behavior of the optical properties as the concentrations of the absorbing and scattering agents are varied. Again several slabs were fabricated and measured using the TCSPC technique described in Section 2.2. First, the concentration of

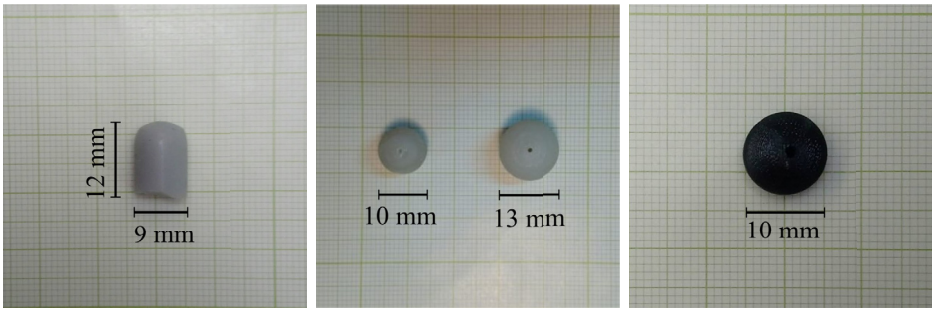

Fig. 6. Examples of the inclusions used to simulate tumor lesions in the phantoms: (a) silicone cylinder, (b) resin spheres, and (c) 3D printed black PLA sphere.

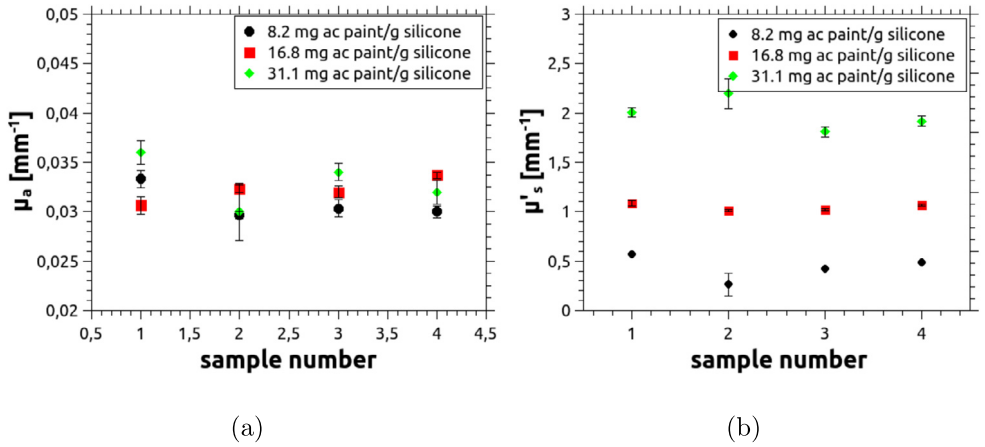

Fig. 7. Optical properties of four independent phantom samples to illustrate the reproducibility achieved with the scattering agent used in this work. Error bars were obtained as the standard deviation of 10 independent measurements, performed on each sample.

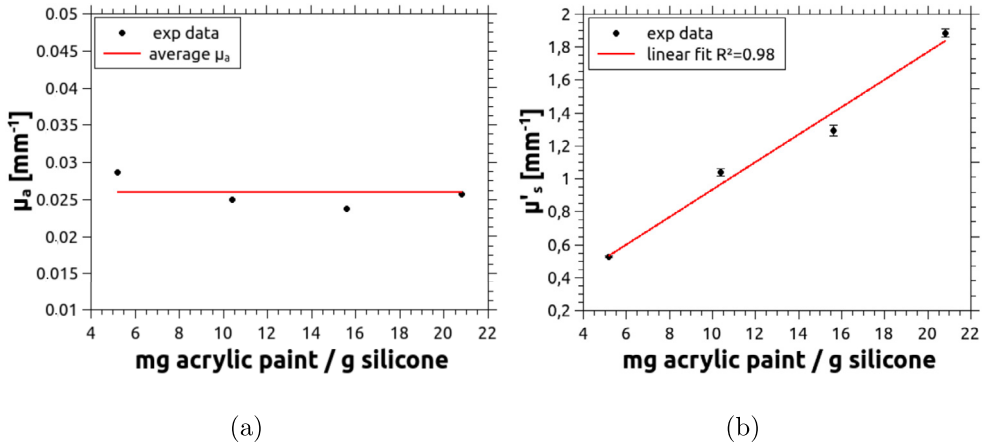

Fig. 8. (a) Absorption coefficient and (b) reduced scattering coefficient of the phantoms vs. concentration of the scattering agent. A well behaved linear increment can be observed beyond the usual range of μ_s' for mammary tissue. Error bars were obtained as the standard deviation of 10 independent measurements, performed on each sample.

the acrylic paint, i.e. the scattering agent, was gradually increased, starting from 4.5 mg of acrylic per gram of mixture, with the addition of 0.39 mg of absorbing agent per gram of silicone. Results, summarized in Fig. 8 (a), show that μ_a remains constant around an average value of 0.026 mm^{-1}. Fig. 8 (b) shows a very good linear behavior in the whole range of acrylic concentration that results in values of μ_s' from below the average for mammary tissue (1 mm^{-1}) and up to about twice this value.

The concentration of the absorbing agent was also varied in an independent set of phantoms, for which the concentration of the scattering agent was kept constant, at 15 mg per gram of silicone. Results are given in Fig. 9, which shows a linear increase of μ_a with increasing toner concentration, while μ_s' shows a slowly decreasing trend. This phenomenon has been observed before [22, 37, 38, 39] with some absorbing agents, and can be explained in terms of particle sizes. In fact, a small fraction of clusters of toner particles, which are larger than the single particles,

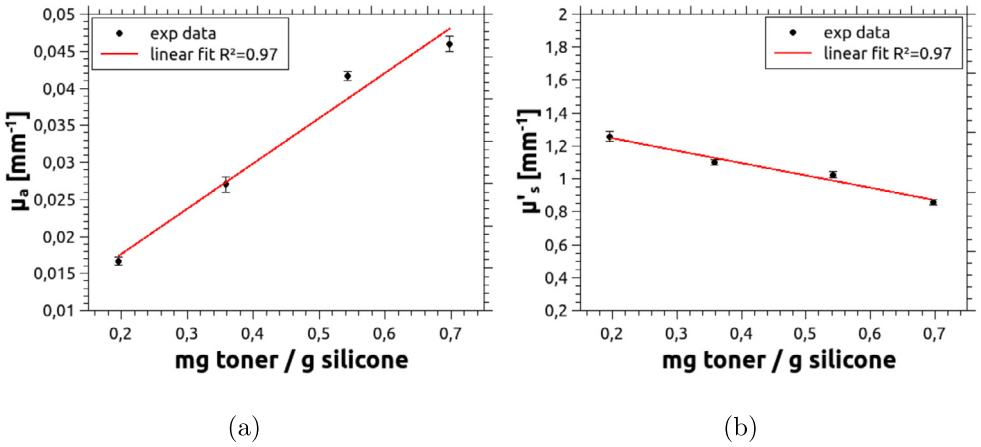

Fig. 9. (a) Absorbing coefficient and (b) reduced scattering coefficient of the phantom vs. toner concentration. The concentration of acrylic is the same in all the phantoms, approximately 15 mg per gram of silicone. Error bars were obtained as the standard deviation of 10 independent measurements, performed on each sample.

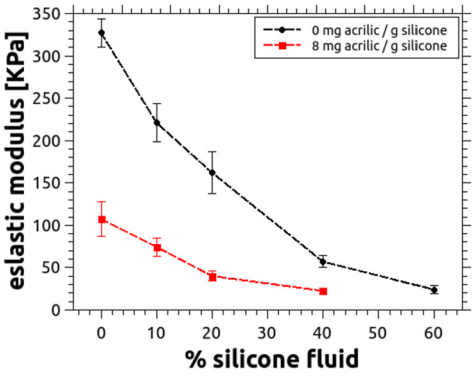

Fig. 10. Elastic modulus as a function of the silicone fluid content, for silicone without acrylic paint (black) and with 8 mg per gram of silicone (red). Error bars are calculated as the standard deviation of five independent measurements. In any case, the content of silicone fluid cannot exceed 70% since beyond this value the mixture will not properly cure.

can occur; these (relatively large particles) obey the Rayleigh scattering and, consequently, their anisotropy factor is increased, thus lowering the global reduced scattering coefficient.

3.2. Mechanical properties

Stress - strain curves were obtained for all samples containing different percentages of silicone fluid, and from them the corresponding elastic moduli were determined as the average value of five independent measurements. Results are shown in Fig. 10.

It is shown that the elastic modulus of silicone decreases with the adding of silicone fluid, but in a non linear fashion. The elastic modulus is also affected by the addition of white acrylic paint, as it can be appreciated in the figure. According to Ramião et al. [30] and Krouskop et al. [40], the fatty and glandular tissues normally present an elastic modulus of approximately 24 kPa, a value that can be reached when the content of silicone fluid is near 60% and no acrylic paint is used. However, since the incorporation of this scattering agent is required, and it further lowers the stiffness of the PDMS, the percentage of fluid must be accordingly reduced. For example, for the amount of paint needed to obtain a scattering coefficient similar to that of a healthy breast, the optimal percentage of silicone fluid drops to 40% (see Fig. 10).

Note that, in some cases, when performing diffuse transmittance experiments, phantoms need to be compressed. This could lead to variations in the optical properties, depending on the degree of compression. To verify if that is the case, we measured the reduced scattering coefficient of a cylindrical phantom as it was stressed between 0 KPa and 40 KPa. This range of compression reduces the thickness of the phantom by a factor of almost 2. For this test, the phantom was constructed with a stiffness reproducing that of a normal breast, i.e. using 40% of silicone fluid. No absorbing agent was added, leaving only the natural absorption of PDMS, which results in $\mu_a \approx 0.0083$ mm^{-1}. The corresponding plot for μ_s' is shown in Fig. 11, in which no significant changes, within the experimental error, were found.

3.3. Imaging experiments

In order to verify if the embedded inclusions are detectable in these types of phantoms, diffuse reflectance and transmittance experiments were performed following the procedures explained previously in Section 2.4. Ultrasound images using a commercial medical device were also obtained for comparison purposes only. Note that, since inclusions emulating tumors were intentionally constructed to be always more absorbing than the surrounding medium, the presence of an inclusion in the imaging experiments produces a region which looks darker than the rest of the imaged area. To give a quantitative criterion for determining the detectability of the lesions, intensity profiles were taken on the final images along a line across them and passing through the diameter of the detected darker region. This allows the calculation of the inclusion visibility as:

$$V = \frac{|I_{Bulk} - I_{Incl}|}{I_{Bulk} + I_{Incl}},$$

where I_{Incl} refers to the minimum intensity value inside the region of the inclusion and I_{Bulk} is the background intensity, far from the inclusion area. With this definition, a value of V close to 1 means that the inclusion is highly detectable, whereas $V \sim 0$ means that it is either barely detectable or not detectable at all. The absolute value in the definition of V allows to include, in the same scale, the visibilities of the ultrasound images, which produce a high intensity value in the synthetic constructed "image" where the inclusion is found.

Cylindrical phantoms - From the analysis of the resulting images, summarized in Table 2, it can be observed that the visibilities produced by C1 are the highest; its inclusion is thus the most easily detectable, regardless of the imaging method used. This is straightforward, since the inclusion is totally absorbing for NIR light, while for ultrasound imaging, as the inclusion was made of a different material (PLA) than the bulk, the speed of sound greatly differs from that of the bulk, also giving a high contrast. Regarding phantom C2, which contains two absorbing inclusions, the resulting visibilities are the lowest for the cylindrical

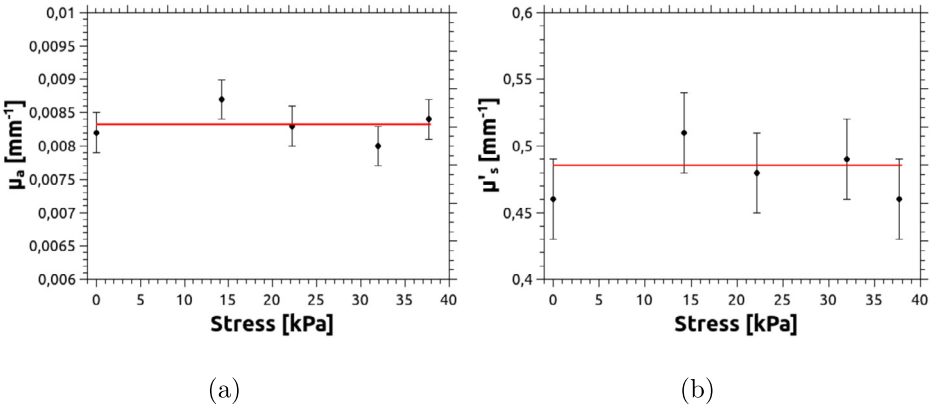

Fig. 11. Optical properties vs compression for a cylindrical phantom. Red lines indicate the average values of μ_a and μ_s'.

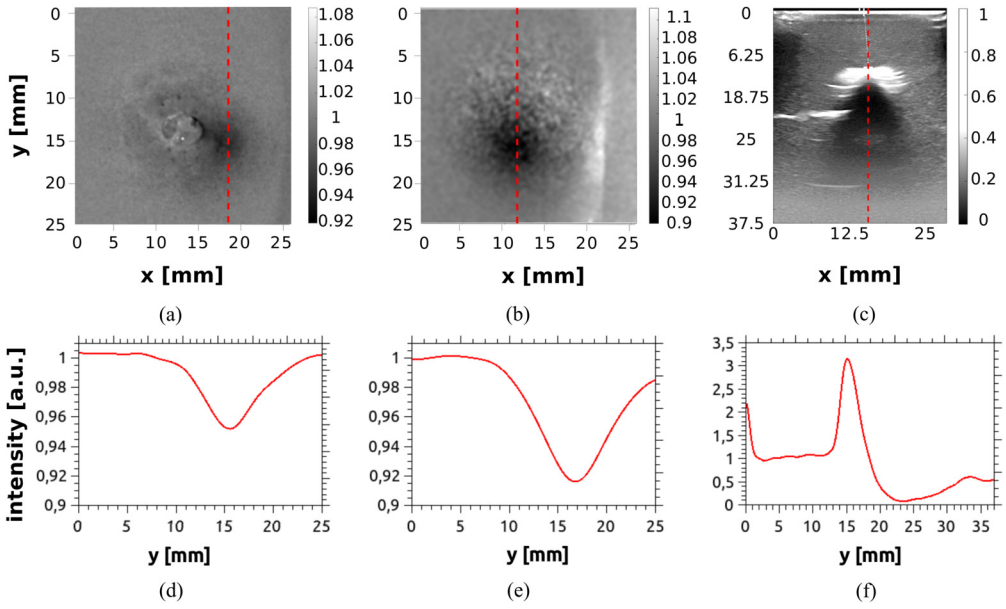

Fig. 12. Images of the phantom A5: (a) DOI in reflectance geometry, (b) DOI in transmittance geometry, and (c) US image. Subplots (d), (e) and (f) show the intensity profiles obtained for each image along the red dashed lines drawn in the respective upper Figures. To obtain smoother profiles, a low-pass filter was applied to all of the images.

Table 2. Visibility of inclusions embedded in the constructed phantoms. All phantoms were tested with DOI and US techniques.

Name	Visibility		
	Reflectance	Transmittance	US
C1	0.09	0.48	0.86
C2	0.02 - ~0	0.01 - ~0	0.33 - 0.38
C3	0.06 - ~0	0.07 - 0.16	0.56 - 0.56
A1	-	-	-
A2	0.1	0.44	0.38
A3	~0	~0	~0
A4	0.01	0.52	~0
A5	0.04 - ~0	0.047 - ~0	0.50 - 0.34

phantoms. The reason for this is that the ratio of the corresponding absorption coefficients is small, namely 1.8 (see Table 1). Opposite to this, for the ultrasound image, the inhomogeneities are still clearly detected because of the different materials that constitute the bulk and the inclusion (PDMS and resin, respectively). Finally, the visibilities of the inclusions in phantom C3 are higher than those in phantom C2, because of the higher absorption ratio, $\mu_{aInclusion}/\mu_{aBulk} = 3.0$, as showed in Table 1; ultrasound images have a good visibility, due to the different materials of the bulk and the inclusion.

Anthropomorphic phantoms - The homogeneous phantom, A1, is not considered in this analysis, since it does not contain any inclusion. For A2, due to the fact that the inclusion is completely black, (much more absorbing than the bulk), and it is made of a different material (PLA) than the bulk, the inclusion is detected with good visibility by each of the three methods, even though it is placed at a depth of 19 mm. The rest of the phantoms, with shape and hardness similar to the human breast, present in general fair visibility, except for phantom A3. For this case the inclusion is not detectable by either of the techniques, since the absorption ratio, $\mu_{aInclusion}/\mu_{aBulk} = 2.3$, is relatively poor for optical contrast and also the inclusion and bulk are made of the same material (poor ultrasound contrast). Phantom A4 has a silicone inclusion as well, which is more absorbing than the bulk and is placed at only 12 mm depth. This results in a good visibility for the transmittance image, although it is barely detected in diffuse reflectance and, as expected, it is not detected by ultrasound imaging. The last anthropomorphic phantom, A5, which contains two resin inclusions, is used to illustrate the whole procedure for assessing the detectability of the inclusions. Results are discussed in detail in the following with the help of Fig. 12. This case constitutes a challenging situation for DOI, since absorption ratios between the inclusions and the bulk are relatively low.

Fig. 12 (a) shows a normalized image of phantom A5 obtained by DOI in reflectance geometry. Only the biggest inclusion (which is also the shallowest) is detected as a dark spot (please refer to Table 1). The corresponding intensity profile shown in Fig. 12 (d) presents only 4% of modulation. For DOI in transmittance geometry, the resulting image is shown in Fig. 12 (b) and its corresponding profile is plotted in (e). Again, only the biggest and shallower inclusion is detected, but now with a better modulation of about 8%. The other inclusion remains undetected. The ultrasound image, Fig. 12 (c) clearly shows the shallowest inclusion with visibility superior to the one achieved by DOI.

Although the main objective of this work is not to compare the goodness of the different imaging methods, the results of this section show that PDMS-based phantoms, either homogeneous or with inclusions, are suitable to be used in DOI experiments. Moreover, if the inclusions are made of a material different from silicone, the phantoms can be also used for ultrasound imaging.

4. Conclusions

In this work we have constructed and validated anthropomorphic breast-shaped phantoms based on PDMS to be used in Diffuse Optical Imaging. Cylindrical phantoms were also made for comparison. Different types of inclusions, emulating lesions, were made and both, their materials and absorption coefficient relative to the bulk were varied.

The mechanical stiffness of the phantoms was also considered as a main parameter. It was shown that the addition of 40% in weight of silicone fluid, together with the corresponding amount of acrylic paint to the PDMS components, reproduces the breast hardness reported in the literature.

TiO_2, which is often used as scattering agent, was replaced by white acrylic paint, showing very good reproducibility and control over the resulting reduced scattering coefficient without the tendency of forming clusters.

Phantoms were validated by both DOI and US and a visibility criterion was introduced to assess the detectability of the simulated lesions. In general, DOI of the cylindrical phantoms shows that embedded lesions with typical volumes of 0.5 cm^3 and with absorption coefficient ratios relative to the bulk of 1.8 or higher can be detected at up to about 10 mm depth. For the case of the anthropomorphic breast phantoms, the fact that they can be compressed reduces the effective depth of the inclusions and thus, lesions were detected for absorption coefficient ratios down to 1.4.

It was also found that, when the inclusions are constructed with a different material than the bulk, they are detectable with ultrasound measurements. This is useful to compare the capability of different techniques when finding potential tumors or cysts.

Declarations

Author contribution statement

V. Noseda Grau; S. Jodra: Conceived and designed the experiments; Performed the experiments; Analyzed and interpreted the data.

H.A. García: Conceived and designed the experiments; Analyzed and interpreted the data; Contributed reagents, materials, analysis tools or data; Wrote the paper.

N.A. Carbone; P. A. Pardini: Contributed reagents, materials, analysis tools or data.

J.A. Pomarico; D.I. Iriarte; D.A. Vera; M.V. Waks Serra: Conceived and designed the experiments; Performed the experiments; Analyzed and interpreted the data; Contributed reagents, materials, analysis tools or data; Wrote the paper.

Funding statement

This research was supported by Fondo para la Investigación Científica y Tecnológica [PICT 2018 Nº 1295 & PICT 2018 Start Up Nº 4709].

Data availability statement

Data will be made available on request.

Declaration of interests statement

The authors declare no conflict of interest.

Additional information

No additional information is available for this paper.

Acknowledgements

Dr. Andrea Berkovic (CIFICEN, UNCPBA - CICPBA - CONICET) for her collaboration with spectroscopic measurements, as well as MD Nicolás De Martino and MD Marina Simoncini, (De Martino Medical Diagnosis, Tandil, Argentina), for the ultrasound images, are gratefully acknowledged.

References

[1] B.J. Tromberg, B.W. Pogue, K.D. Paulsen, A.G. Yodh, D.A. Boas, A.E. Cerussi, Assessing the future of diffuse optical imaging technologies for breast cancer management, Med. Phys. 35 (6) (2008) 2443–2451.

[2] A.P. Gibson, J.C. Hebden, S.R. Arridge, Recent advances in diffuse optical imaging, Phys. Med. Biol. 50 (4) (2005) R1–R43.

[3] R. Choe, A. Corlu, K. Lee, T. Durduran, S.D. Konecky, M. Grosicka-Koptyra, S.R. Arridge, B.J. Czerniecki, D.L. Fraker, A. DeMichele, B. Chance, M.A. Rosen, A.G. Yodh, Diffuse optical tomography of breast cancer during neoadjuvant chemotherapy: a case study with comparison to MRI, Med. Phys. 32 (4) (2005) 1128–1139.

[4] L. Hou, Y. Liu, L. Qian, Y. Zheng, J. Gao, W. Cao, Y. Shang, Portable near-infrared technologies and devices for noninvasive assessment of tissue hemodynamics, J. Healthc. Eng. 2019 (2019).

[5] P. Taroni, A.M. Paganoni, F. Ieva, A. Pifferi, G. Quarto, F. Abbate, E. Cassano, R. Cubeddu, Non-invasive optical estimate of tissue composition to differentiate malignant from benign breast lesions: a pilot study, Sci. Rep. 7 (August 2016) (2017) 40683.

[6] G. Quarto, L. Spinelli, A. Pifferi, A. Torricelli, R. Cubeddu, F. Abbate, N. Balestreri, S. Menna, E. Cassano, P. Taroni, Estimate of tissue composition in malignant and benign breast lesions by time-domain optical mammography, Biomed. Opt. Express 5 (10) (2014) 3684–3698.

[7] M. Kleshnin, A. Orlova, M. Kirillin, G. Golubiatnikov, I. Turchin, A technique for measuring oxygen saturation in biological tissues based on diffuse optical spectroscopy, in: Optics InfoBase Conference Papers Part F61-ECBO 2017, 2017, pp. 1–7.

[8] Y. Hoshi, Y. Yamada, Overview of diffuse optical tomography and its clinical applications, J. Biomed. Opt. 21 (9) (2016) 091312.

[9] Y. Ueda, K. Yoshimoto, E. Ohmae, T. Suzuki, T. Yamanaka, D. Yamashita, H. Ogura, C. Teruya, H. Nasu, E. Ima, H. Sakahara, M. Oda, Y. Yamashita, Time-resolved optical mammography and its preliminary clinical results, Technol. Cancer Res. Treat. 10 (5) (2011) 393–401.

[10] P. Taroni, A. Torricelli, L. Spinelli, A. Pifferi, F. Arpaia, G. Danesini, R. Cubeddu, Time-resolved optical mammography between 637 and 985 nm: clinical study on the detection and identification of breast lesions, Phys. Med. Biol. 50 (11) (2005) 2469–2488.

[11] D. Grosenick, A. Hagen, O. Steinkellner, A. Poellinger, S. Burock, P.M. Schlag, H. Rinneberg, R. Macdonald, A multichannel time-domain scanning fluorescence mammograph: performance assessment and first in vivo results, Rev. Sci. Instrum. 82 (2) (2011) 024302.

[12] P.G. Anderson, S. Kalli, A. Sassaroli, N. Krishnamurthy, S.S. Makim, R.A. Graham, S. Fantini, Optical mammography in patients with breast cancer undergoing neoadjuvant chemotherapy: individual clinical response index, Acad. Radiol. 24 (10) (2017) 1240–1255.

[13] D. Grosenick, H. Rinneberg, R. Cubeddu, P. Taroni, Review of optical breast imaging and spectroscopy, J. Biomed. Opt. 21 (9) (2016) 091311.

[14] G. Maffeis, E. Ferocino, A.D. Mora, A. Pifferi, R. Cubeddu, P. Taroni, In vivo test-driven upgrade of a time domain multi-wavelength optical mammograph, Biomed. Opt. Express 12 (2) (2021) 1105.

[15] A. Pifferi, A. Torricelli, A. Bassi, P. Taroni, R. Cubeddu, H. Wabnitz, D. Grosenick, M. Möller, R. Macdonald, J. Swartling, T. Svensson, S. Andersson-Engels, R.L.P. van Veen, H.J.C.M. Sterenborg, J.-m. Tualle, H.L. Nghiem, S. Avrillier, M. Whelan, H. Stamm, Performance assessment of photon migration instruments: the MEDPHOT protocol, Appl. Opt. 44 (11) (2005) 2104–2114.
[16] B.W. Pogue, M.S. Patterson, Review of tissue simulating phantoms for optical spectroscopy, imaging and dosimetry, J. Biomed. Opt. 11 (4) (2006) 041102.
[17] A. Pifferi, A. Torricelli, R. Cubeddu, G. Quarto, R. Re, S.K.V. Sekar, L. Spinelli, A. Farina, F. Martelli, H. Wabnitz, Mechanically switchable solid inhomogeneous phantom for performance tests in diffuse imaging and spectroscopy, J. Biomed. Opt. 20 (12) (2015) 121304.
[18] H. Wabnitz, D.R. Taubert, T. Funane, M. Kiguchi, H. Eda, A. Pifferi, A. Torricelli, R. Macdonald, Characterization of homogeneous tissue phantoms for performance tests in diffuse optics, in: Design and Quality for Biomedical Technologies IX, vol. 9700, 2016, p. 970004.
[19] F. Ayers, A. Grant, D. Kuo, D.J. Cuccia, A.J. Durkin, Fabrication and characterization of silicone-based tissue phantoms with tunable optical properties in the visible and near infrared domain, in: Design and Performance Validation of Phantoms Used in Conjunction with Optical Measurements of Tissue, vol. 6870, International Society for Optics and Photonics, 2008, p. 687007.
[20] R.B. Saager, A. Quach, R.A. Rowland, M.L. Baldado, A.J. Durkin, Low-cost tissue simulating phantoms with adjustable wavelength-dependent scattering properties in the visible and infrared ranges, J. Biomed. Opt. 21 (6) (2016) 067001.
[21] S. Jiang, B.W. Pogue, T.O. McBride, M.M. Doyley, S.P. Poplack, K.D. Paulsen, Near-infrared breast tomography calibration with optoelastic tissue simulating phantoms, J. Electron. Imaging 12 (4) (2003) 613–620.
[22] A.M. Goldfain, P. Lemaillet, D.W. Allen, K.A. Briggman, J. Hwang, Polydimethylsiloxane tissue-mimicking phantoms with tunable optical properties, J. Biomed. Opt. 27 (07) (2021) 1–13.
[23] M.V. Waks Serra, N.A. Carbone, H.O. Di Rocco, H.A. García, D.I. Iriarte, J.A. Pomarico, H.F. Ranea-Sandoval, Diffuse light transmission profiles obtained using CW: a comparative analysis with time resolved experiments, Optik, Int. J. Light Electron Opt. 125 (14) (2014) 3507–3513.
[24] M.V. Waks Serra, D. Grosenick, R. Macdonald, J.A. Pomarico, D.I. Iriarte, A systematic study on fluorescence contrast in near infrared diffuse transmittance imaging with indocyanine green, J. Near Infrared Spectrosc. (2019).
[25] H.G. Akarçay, S. Preisser, M. Frenz, J. Rička, Determining the optical properties of a gelatin-tio 2 phantom at 780 nm, Biomed. Opt. Express 3 (3) (2012) 418–434.
[26] R. Cubeddu, A. Pifferi, P. Taroni, A. Torricelli, G. Valentini, A solid tissue phantom for photon migration studies, Phys. Med. Biol. 42 (10) (1997) 1971.
[27] J. Hwang, H.-J. Kim, P. Lemaillet, H. Wabnitz, D. Grosenick, L. Yang, T. Gladytz, D. McClatchy, D. Allen, K. Briggman, B. Pogue, Polydimethylsiloxane tissue-mimicking phantoms for quantitative optical medical imaging standards, in: Design and Quality for Biomedical Technologies X, vol. 10056, 2017, p. 1005603.
[28] A. Technologies, Optically clear silicone [Online]. https://albrightsilicone.com/optically-clear-silicone-molding/, 2020. (Accessed 18 March 2021).
[29] T. Vo-Dinh (Ed.), Biomedical Photonics Handbook, CRC Press, 2003.
[30] N.G. Ramião, P.S. Martins, R. Rynkevic, A.A. Fernandes, M. Barroso, D.C. Santos, Biomechanical properties of breast tissue, a state-of-the-art review, Biomech. Model. Mechanobiol. 15 (5) (2016) 1307–1323.
[31] S. Schieck, Herstellung und Charakterisierung strukturierter, gewebeähnlicher Phantome für die biomedizinische Optik, Ph.D. thesis, Fachbereiches Ingenieurwesen/Wirtschaftsingenieurwesen der Technischen Fachhochschule Wildau, 2005.
[32] N.A. Carbone, G. Baez, H.A. García, M.V. Waks Serra, H.O. Di Rocco, D.I. Iriarte, J.A. Pomarico, D. Grosenick, R. Macdonald, Diffuse reflectance optical topography: location of inclusions in 3D and detectability limits, Biomed. Opt. Express 5 (5) (2014) 1336–1354.
[33] P.A. Pardini, M.V. Waks Serra, H.F. Ranea-Sandoval, J.A. Pomarico, D.I. Iriarte, Study of inks used in biomedical optics phantoms: stability and ageing, J. Near Infrared Spectrosc. 23 (4) (2015) 219.
[34] D. Contini, F. Martelli, G. Zaccanti, Photon migration through a turbid slab described by a model based on diffusion approximation. i. Theory, Appl. Opt. 36 (19) (1997) 4587–4599.
[35] G. Lamouche, B.F. Kennedy, K.M. Kennedy, C.-E. Bisaillon, A. Curatolo, G. Campbell, V. Pazos, D.D. Sampson, Review of tissue simulating phantoms with controllable optical, mechanical and structural properties for use in optical coherence tomography, Biomed. Opt. Express 3 (6) (2012) 1381.
[36] H.M. Ismail, C.G. Pretty, M.K. Signal, M. Haggers, C. Zhou, J.G. Chase, Mechanical behaviour of tissue mimicking breast phantom materials, Biomed. Phys. Eng. Express 3 (4) (2017) 045010.
[37] A. Rehman, I. Ahmad, K. Rehman, S. Anwar, S. Firdous, M. Nawaz, Optical properties measurement of highly diffusive tissue phantoms for biomedical applications, Laser Phys. 25 (2) (2014) 025605.
[38] S.J. Madsen, M.S. Patterson, B.C. Wilson, The use of India ink as an optical absorber in tissue-simulating phantoms, Phys. Med. Biol. 37 (4) (1992) 985–993.
[39] P. Di Ninni, F. Martelli, G. Zaccanti, The use of India ink in tissue-simulating phantoms, Opt. Express 18 (26) (2010) 26854–26865.
[40] T.A. Krouskop, T.M. Wheeler, F. Kallel, B.S. Garra, T. Hall, Elastic moduli of breast and prostate tissues under compression, Ultrason. Imag. 20 (4) (1998) 260–274.